

Measuring the radial elasticity of carbon nanotube yarns

Enlai Gao

Department of Engineering Mechanics, School of Civil Engineering, Wuhan University, Wuhan, Hubei, 430072, China



ARTICLE INFO

Article history:

Received 16 June 2019

Received in revised form

28 September 2019

Accepted 13 October 2019

Available online 15 October 2019

ABSTRACT

Carbon nanotube yarn, one of the most important macroscopic architectures of carbon nanotubes, displays ultrahigh stiffness in axial direction yet remarkable softness in the radial deformation. However, in contrast to the axial mechanical behavior that has been extensively studied, the mechanical response to load applied in the radial direction, which is of fundamental importance to perform the material functions, was less explored. In this work, an experimental approach is developed to measure the radial elastic modulus of the carbon nanotube yarns with microscopic mechanisms elucidated by theoretical analysis. It is found that the measured radial elastic modulus increases with the increasing of the cycle loading number and the twist density of the carbon nanotube yarns, suggesting the tunability of the radial elasticity of carbon nanotube yarn by mechanical loading. Furthermore, a hierarchical model is proposed to explain the abovementioned structure-property relationship, revealing that the curly, entangled, locally bundling nature strongly modulates the radial elastic modulus of the carbon nanotube yarns. This work not only provides essential insight in the radial deformability of carbon nanotube yarns, but also develops a method that could be applied to measure the radial mechanical properties of other micro-fibers.

© 2019 Elsevier Ltd. All rights reserved.

1. Introduction

The development of high-performance, light-weight, and multifunctional fibrous materials has been continuously driven by the increasing industrial demands for aerospace, civil and other related applications. Recent advances in large-scale synthesis of high-quality sp^2 carbon nanostructures such as carbon nanotubes (CNTs) and graphene open new dimensions of material design from the bottom up [1–5]. In the view of mechanical performance, CNT is a promising candidate for constructing fibrous materials as it provides exceptional tensile stiffness and strength. The one-dimensional tubular geometry and inter-tube cohesion naturally promote the assembling process of CNTs into carbon nanotube yarn (CNTY) [6] that is an oriented assembly of CNTs with exceptional axial mechanical performance benefiting from the strong covalent carbon-carbon bonds [7]. Diverse applications of CNTYs have been proposed, such as reinforcing composites, artificial muscles, energy harvester [8–12]. In most of the aforementioned applications, the radial deformation mode plays an essential role in fulfilling the material functions.

For CNT, the axial elastic modulus is in the order of 1000 GPa,

while the radial elastic modulus is only about 30 GPa [13,14]. Similarly, the radial elastic modulus of CNTYs is expected to be much softer than the axial one (in the order of 10–100 GPa) [15]. For example, evidence for the softness of CNTYs in the radial direction has been reported in experiments of CNTYs under twist-induced pressure [11]. The axial tensile properties of CNTYs have been widely studied. Furthermore, Zu et al. recently measured the axial compressive properties of CNTYs using the tensile recoil measurement [16]. However, compared with these axial mechanical properties of CNTYs that have been well studied, the mechanical resistance of CNTYs to radial loads, which is fundamentally important to enable material functions, was less explored. Mechanical test on CNTYs in the radial direction is challenging for the small diameter and remarkable roughness of CNTYs. By performing transverse compression, Li et al. first measured the radial mechanical properties of CNTYs, which capture a nonlinear and inelastic behavior [17]. While considering the microstructural complexity of CNTYs that may be affected by varying factors, such as, twist density and cycle loading, a comprehensive understanding as well as a quantitative modelling of the radial deformability of CNTYs is fundamental as well as highly desirable.

In this work, we developed a compression test to measure the radial elasticity of CNTYs. The radial elastic moduli of CNTYs with different twist densities under different numbers of cycle loading

E-mail address: enlaigao@whu.edu.cn.

are extracted from the experimental measurements by applying the extension of the Hertz model, which are compared favorably with natural rubber. The radial stiffness increases with the increasing of twist density and cycle loading number, suggesting the radial elasticity can be efficiently modulated by mechanical twist and cycle loadings. Finally, theoretical analysis was performed to capture the essential physics of radial elasticity, which reveals that the soft radial deformability of CNTYs mainly results from their wavy and loose structures.

2. Materials and methods

2.1. Fabrication and microstructures of CNTYs

CNTYs were prepared from carbon multi-walled nanotubes (MWNTs) drawn from MWNT forests with the height of about 300 μm . Scanning electron microscope (SEM) images and transmission electron microscope (TEM) showed that the outer diameter of MWNTs with about 8 walls is about 10 nm, although there is considerable size dispersion of MWNTs. For the fabrication of CNTYs, MWNT sheets were drawn from the forest and then assembled into a 20-cm-long and 4-cm-wide sheet stack with MWNTs aligned along the length direction. Afterwards, each end of a MWNT sheet stack was attached by an adhesive tape and then manually rolled the stack into a MWNT cylinder. The cylinder attaching to a motor at its top was then suspended vertically by applying about 30 MPa of stress at the bottom end. We inserted twist along the central axis of this cylinder from its top end while preventing the rotation of its bottom end, thus enabling investigation of the effects of twist density on the radial elasticity of CNTYs. More details of the growth of CNTs and preparation of CNTYs can be found in our previous work [11].

2.2. Radial elastic modulus characterized by compression experiments

Samples of length 1 cm were cut from the prepared CNTYs by a razor blade. The diameter of each CNTY sample was measured by SEM before the sample was tested under radial compression. Two CNTY samples were placed parallelly on one wafer substrate with a separation distance of about 0.5 cm and then covered with another slice of wafer. Note here that the sample ends were attached on substrate by tapes to prevent the untwist of CNTYs. As the wafers were estimated to be far stiffer than CNTYs, the deformations of wafers in these tests were neglected. We used a diamond flat punch with diameter of 100 μm as a compression platen in all tests. The compressive load applied by the flat punch was transferred through the top layer of wafer, thus resulting in a radial deformation configuration of compressed CNTYs between two plates. All the compression experiments were performed with constant loading rate of 2 mN/s to ensure quasi-static loading, and the maximum compressive force of 200 mN was applied. We cleaned the diamond flat punch before testing, and prepared and stored the samples in the clean-room facility to reduce the effect of other particles. This procedure was adopted in all the experiments.

The set-up in our micro-compression tests can be modeled as a cylinder compressed between plates. For this model, an equation to calculate the apparent radial elastic modulus of the cylinder based on an extension of Hertz elastic theory [18] could be given

$$E_r = 8FZ^2(1-\nu^2)/\pi D l \quad (1)$$

where F is the applied normal load, l , D , E_r and ν are the contact length, the diameter of the cylindrical body, Young's modulus and Poisson's ratio of the cylindrical body, respectively, and Z is given as

$$Z = D/w \quad (2)$$

where w is the width of the contact region while challenging to measure. Thus, Z can be determined by

$$\Delta/D = [1/(2Z^2)][\ln(2Z)+1/2] \quad (3)$$

where Δ is the vertical deformation of the cylinder. Combined with Eqs. (1)–(3), the radial elastic moduli were extracted from experimental measurements using the following procedures:

1. Measure the diameter of CNTY (D) before compression and then record the force-deformation (F - Δ) curve in compression tests;
2. Calculate the $1/Z^2$ from the measured Δ and D using Eq. (3);
3. Obtain the radial elastic modulus E_r by fitting Eq. (1) to F - $1/Z^2$ data.

It should be noted that the Poisson's ratio of CNTYs is orientation-dependent because of elastic anisotropy. Miao et al. demonstrated that the axial Poisson's ratio (the negative ratio between transverse strain and axial strain under the axial loading) can be tuned over an extremely wide range of values, resulting from their highly variable porosity of the yarn structure [19]. Similarly, the Poisson's ratio in the cross-section (the negative ratio between transverse strain and radial strain under the radial loading) used in our model is expected to depend on the different microstructures of CNTYs. Here 0.3 as the mean value of common materials is adopted in our calculation because of the challenge in measuring the Poisson's ratio in the cross-section. Therefore, it should be noted that if the actual Poisson's ratio is larger than 0.3, the extracted radial elastic modulus is overestimated. Otherwise, it is underestimated.

3. Results and discussion

3.1. Typical mechanical responses of CNTYs under radial loads

As illustrated in Fig. 1a, we first probed the radial deformation of a CNTY sample with a diameter of 166 μm and twist density of 750 turns/m under radial loads by using micro-compression tests (Sample details are summarized in Table 1). The typical morphology and force-displacement (F - Δ) curve of a CNTY (the displacement is that under the load) are shown in Fig. 1b–c. We can find that the force initially increases with the deformation slowly, and then almost linearly increases with the deformation. It could be inferred that the initial non-linear behavior of the CNTY under radial compression is attributed to the flattening of the surface asperities of the CNTY, which is also observed in similar radial compression tests on other cylindrical materials [20].

3.2. Effect of cycle and twist loading on the radial elastic modulus of CNTYs

Furthermore, we explored the radial deformation behaviors of CNTYs with varying twist densities under cycle loading. Fig. 2 shows that the radial elastic modulus of CNTYs depends greatly on the cycle number. The values of the radial elastic modulus increase initially and then converge to a steady value as the cycle number increases. The CNTYs with twist density of 750 turns/m display an increasing radial elastic modulus up to 65.0% (from 12.3 MPa to 20.3 MPa) in response to cycle load of 200 mN amplitude for ten times. Test of CNTYs with higher twist density of 1500 turns/m also exhibited a similar effect (32.4% increasing of the radial elastic modulus from 22.2 MPa to 29.4 MPa), implying that the stiffening behavior resulting from cycle loading is independent of the special experimental samples used.

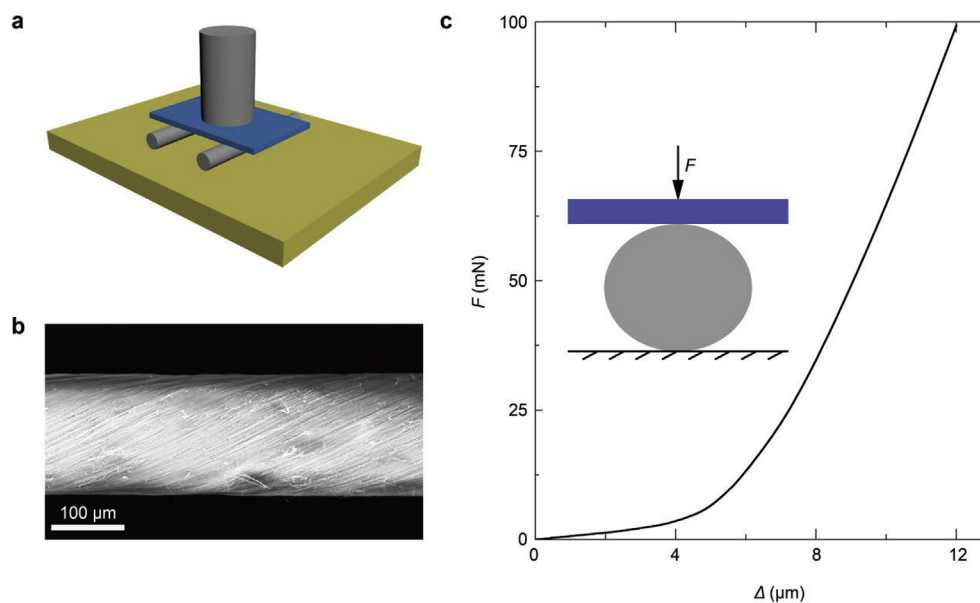


Fig. 1. Measurement of the radial elasticity of CNTYs. (a) Illustration of experimental set-up, where two CNTYs are placed between two slices of wafers. (b) SEM image of the typical CNTY. (c) Typical force-deformation curve and cross-sectional view of a illustrated radially compressed CNTY. (A colour version of this figure can be viewed online.)

Table 1
Details for the measured CNTY samples.

sample	twist density (turns/m)	diameter (μm)	twist angle ($^\circ$)	density (g/cm^3)	E_r at 1st loading (MPa)	E_r at 10th loading (MPa)
1	750	166	21.4	0.8	12.3	20.3
2	1500	116	28.7	1.1	22.2	29.4

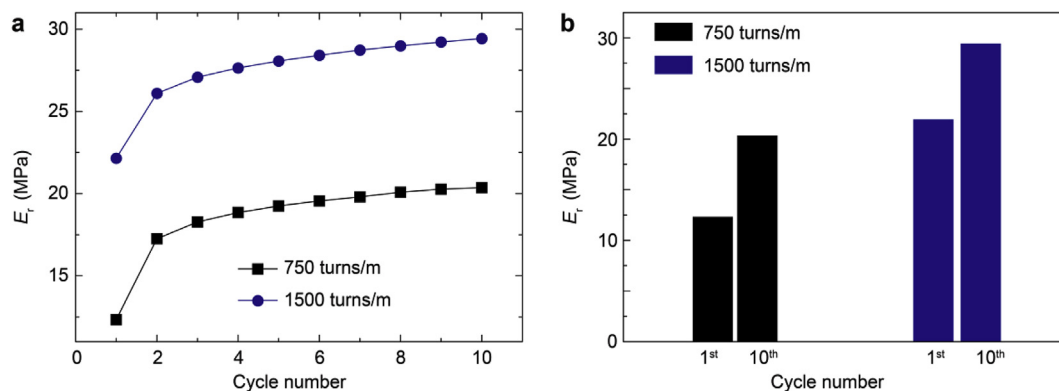


Fig. 2. Radial elastic modulus of CNTYs. (a) The radial elastic modulus for CNTYs with varying twist densities under cycle loading. (b) The comparison of the radial elastic modulus measured for CNTYs with different twist densities under the 1st and 10th cycle number (Sample details can be found in Table 1).

Meanwhile, it should be noted that, as summarized in Table 1, the values of radial elastic modulus increase as the twist density increases, suggesting the tunability of the radial stiffness of CNTYs by twist loading. More specifically, the initial (steady) values of radial elastic moduli go up from 12.3 (20.3) MPa to 22.2 (29.4) MPa for CNTYs with twist density of 750 turns/m and 1500 turns/m, respectively. In addition, the initial (steady) values of specific radial elastic moduli of CNTYs with twist densities of 750 and 1500 turns/m are calculated as 15.4 (25.4) and 20.2 (26.7) MPa/(g/cm³) from the corresponding radial elastic moduli and densities as shown in Table 1, indicating that the specific radial elastic moduli of CNTYs also increase with both twist density and cycle number of loading. Similar to the previous observation of strain hardening behavior of polymer nanocomposites, liquid crystal elastomers, and graphene

films under dynamical loading [21–23], the microstructure-evolution-induced radial stiffening in CNTYs could be effectively actuated once applying mechanical twist and cycle loadings, the underlying mechanism of which will be discussed later. In addition, it could be found that, in contrast to the axial Young's modulus of CNTYs in the order of 10–100 GPa, the radial elastic modulus of the CNTYs is about 3–4 orders lower than axial one (Fig. 3), suggesting the extreme elastic anisotropy as well as ultra-soft nature of radial deformation in CNTYs and thus there are plenty room in CNTYs to endow the material with multifunction.

3.3. Theoretical analysis

To elucidate the correspondence between the mechanical

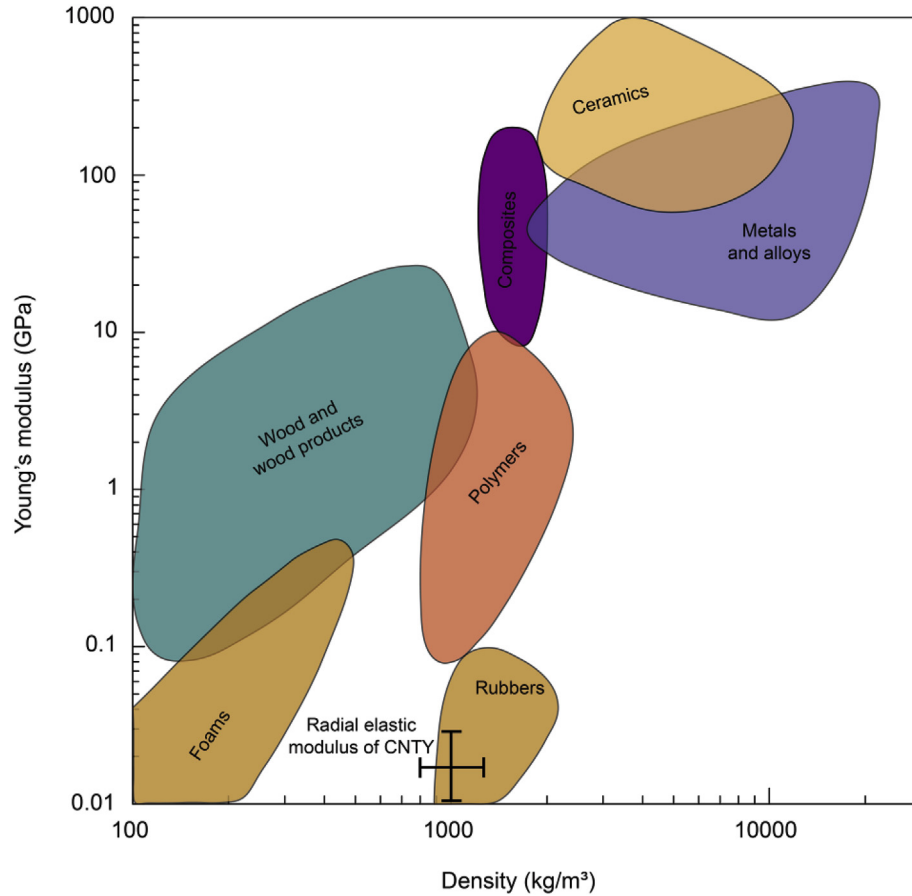


Fig. 3. Illustration of Young's moduli versus densities of material selection charts [24], compared with radial elastic moduli of CNTYs. (A colour version of this figure can be viewed online.)

responses of CNTYs under radial loading and their microstructures, we constructed a theoretical model for the CNTYs based on experimental evidence. Specifically, based on TEM and SEM images of the cross-section and the longitudinal section morphologies of CNTYs (Fig. 4a–b), the microstructures of CNTYs are illustrated in Fig. 4c, consisting of inter-connected bundles (with averaged about 25 MWNTs per bundle). The bundles branch out (forking) and merge in (bundling) throughout the assemblies, making an extended, inherently interconnected network [25]. The microstructural evolution under radial loading involves compressing the solid region of closely packing MWNT shells like graphite as well as deforming the hollow region in bundles and inter-bundles. Therefore, the contributions on the radial stiffness of CNTYs could be divided into two parts, that are (1) solid region of closing packing CNT shells and (2) hollow region including void spacing in bundles and inter-bundles. Compared to the compressive deformation of the solid region, the hollow region in the CNTYs is stabilized by its microstructural hierarchy of bending, folding and wrinkling and thereby could exhibit much lower stiffness, which is expected to dominate the radial softness of CNTYs especially with low density. With these arguments, we rationalize the mechanisms through a Reuss model to infer the effective elastic modulus of the CNTYs. In the model (Fig. 4d), the two sets of springs represent the elasticity of the solid region (spring 1) and hollow region (spring 2), respectively. The stiffnesses of these two springs (k_{1-2}) as well as their overall stiffness (k) are given as

$$k_1 = E_1 A / L_1 \quad (4)$$

$$k_2 = E_2 A / L_2 \quad (5)$$

$$k = k_1 k_2 / (k_1 + k_2) = E_r A / (L_1 + L_2) \quad (6)$$

where E_{1-2} and L_{1-2} are the Young's moduli and lengths of the springs 1–2 that share the same equivalent cross-section area A , respectively. In addition, $V_1 = A \times L_1$, $V_2 = A \times L_2$, and $V = A \times (L_1 + L_2)$ are the equivalent volumes of springs 1–2, and their overall volume, respectively. The overall density is $\rho = (\rho_1 V_1 + \rho_2 V_2) / V$, where ρ_1 and ρ_2 are the densities of solid and hollow regions, respectively. Since the structures of closing packing MWNT shells are similar to the structures of graphite and the hollow regions are assumed to be massless, thus $\rho_1 = 2.26 \text{ g/cm}^3$ and $\rho_2 = 0 \text{ g/cm}^3$ were adopted in this analysis. Combining Eqs. (4)–(6), the radial elastic modulus E_r is derived as

$$E_r = E_1 E_2 / [E_1 (1 - \rho / \rho_1) + E_2 \rho / \rho_1] \quad (7)$$

Unlike the constant value of E_1 (36.5 GPa for graphite) [26], E_2 could be expected to increase with the overall density (ρ) increasing. Without loss of generality, here we assumed that $E_2 = c(\rho / \rho_1)^n$, where c is a pre-factor and n is the power-law coefficient. Hence, Eq. (7) can be rewritten as

$$E_r = E_1 c (\rho / \rho_1)^n / [E_1 (1 - \rho / \rho_1) + c (\rho / \rho_1)^{n+1}] \quad (8)$$

Eq. (8) is a two-parameter function with definite physical meaning, which was used to fit the experimental data. Combining

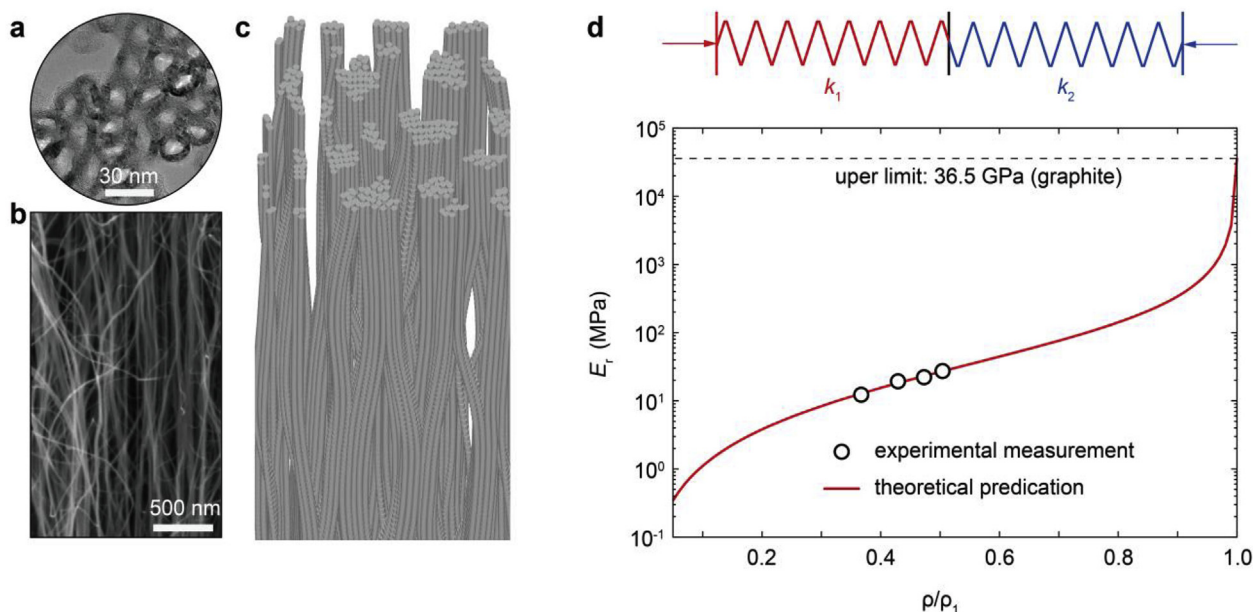


Fig. 4. Experimental characterization and modelling of the microstructures of CNTYs, and the theoretical analysis of radial elasticity of CNTYs with their microstructures. (a) TEM image of the cross-section [11] and (b) SEM image of the longitudinal section of CNTY. (c) Modelling the CNTY based on the experimental characterization. (d) The theoretical model and prediction of radial elastic modulus of CNTYs as a function of material density (Each experimental data was measured from one sample with a specific density). (A colour version of this figure can be viewed online.)

Eq. (8) and experimental measurement of ρ and E_r of CNTYs, the parameters c and n are calculated as 40.6 MPa and 1.6, respectively, and the theoretical prediction is given in Fig. 4d. With the extension of the theory, radial elasticity of CNTYs with a wide range of densities is predicted as shown in Fig. 4d, where the upper limit is 36.5 GPa for graphite with a density of 2.26 g/cm^3 [26]. From these analysis and prediction, one could expect to enhance the radial rigidity of CNTYs by improving either their packing and alignment to increase the density (ρ) of CNTYs, or inter-tube, inter-bundle interactions and topologies (for example, by chemical crosslinks or irradiations) to increase the stiffness of hollow region (c , n). This explanation could be also given to CNTYs under cycle loading. With these improvements, the mechanical resistance of radial deformation of CNTYs could be enhanced.

4. Conclusion

In summary, an experimental approach is developed to probe the radial elasticity of CNTYs by considering their microstructural characteristics. Ultra-soft radial moduli of CNTYs are measured, suggesting the ultra-soft nature of radial deformability of CNTYs and thus there are plenty room in CNTYs to fill the material functions. The curvy, entangled, locally bundling morphologies of CNTs strongly modulate the radial elasticity of their yarns, reducing the apparent radial elastic modulus significantly. The underlying mechanism is elucidated by analyzing microstructural evolution in the CNTYs. This work not only provides a quantitative understanding of the radial deformability of CNTYs, but also provides methods to tune their microstructures as well as the radial elasticity by mechanical twist and cycle loading.

Declaration of competing interest

The Author declares no Competing Financial or Non-Financial Interests.

Acknowledgements

This work was supported by the National Natural Science Foundation of China (11902225), the Natural Science Foundation of Hubei Province (2019CFB174), the Fundamental Research Funds for the Central Universities (413000091), and the Starting-up Fund of Wuhan University. E.G. thanks Lintec of America, Nano-Science and Technology Center for providing CNT forests, the early technological assistance in experiments from Tingge Xu and Xinghao Hu, and the helpful discussion with Ray Baughman, and Dong Qian.

Appendix A. Supplementary data

Supplementary data to this article can be found online at <https://doi.org/10.1016/j.carbon.2019.10.033>.

References

- [1] N. Behabtu, C. Young, D. Tsentelovich, O. Kleinerman, X. Wang, A. Ma, E. Bengio, R.F. ter Waarbeek, J. de Jong, R. Hoogerwerf, S. Fairchild, J. Ferguson, B. Maruyama, J. Kono, Y. Talmon, Y. Cohen, M. Otto, M. Pasquali, Strong, light, multifunctional fibers of carbon nanotubes with ultrahigh conductivity, *Science* 339 (6116) (2013) 182–186.
- [2] Y. Hao, M. Bharathi, L. Wang, Y. Liu, H. Chen, S. Nie, X. Wang, H. Chou, C. Tan, B. Fallahzad, H. Ramanarayan, C. Magnuson, E. Tutuc, B. Yakobson, K. McCarty, Y. Zhang, P. Kim, J. Hone, L. Colombo, R. Ruoff, The role of surface oxygen in the growth of large single-crystal graphene on copper, *Science* 342 (6159) (2013) 720–723.
- [3] Z. Xu, H. Sun, X. Zhao, C. Gao, Ultrastrong fibers assembled from giant graphene oxide sheets, *Adv. Mater.* 25 (2) (2013) 188–193.
- [4] E. Gao, S. Lin, Z. Qin, M. Buehler, X. Feng, Z. Xu, Mechanical exfoliation of two-dimensional materials, *J. Mech. Phys. Solids* 115 (2018) 248–262.
- [5] Y. Wen, E. Gao, Z. Hu, T. Xu, H. Lu, Z. Xu, C. Li, Chemically modified graphene films with tunable negative Poisson's ratios, *Nat. Commun.* 10 (1) (2019) 2446.
- [6] M. Zhang, K. Atkinson, R. Baughman, Multifunctional carbon nanotube yarns by downsizing an ancient Technology, *Science* 306 (5700) (2004) 1358–1361.
- [7] B. Yakobson, P. Avouris, Mechanical properties of carbon nanotubes, in: M.S. Dresselhaus, G. Dresselhaus, P. Avouris (Eds.), *Carbon Nanotubes: Synthesis, Structure, Properties, and Applications*, Springer, 2001, pp. 287–327.
- [8] K. Koziol, J. Vilatela, A. Moisala, M. Motta, P. Cuniff, M. Sennett, A. Windle, High-performance carbon nanotube fiber, *Science* 318 (5858) (2007) 1892–1895.
- [9] C. Haines, M. Lima, N. Li, G. Spinks, J. Foroughi, J. Madden, S. Kim, S. Fang,

- M. Jung de Andrade, F. Goktepe, O. Goktepe, S. Mirvakili, S. Naficy, X. Lepro, J. Oh, M. Kozlov, S. Kim, X. Xu, B.J. Swedlove, G. Wallace, R. Baughman, Artificial muscles from fishing line and sewing thread, *Science* 343 (6173) (2014) 868–872.
- [10] M. De Volder, S. Tawfick, R. Baughman, A. Hart, Carbon nanotubes: present and future commercial applications, *Science* 339 (6119) (2013) 535–539.
- [11] S. Kim, C. Haines, N. Li, K. Kim, T. Mun, C. Choi, J. Di, Y. Oh, J. Oviedo, J. Bykova, S. Fang, N. Jiang, Z. Liu, R. Wang, P. Kumar, R. Qiao, S. Priya, K. Cho, M. Kim, M. Lucas, L. Drummy, B. Maruyama, D. Lee, X. Lepro, E. Gao, D. Albarq, R. Ovalle-Robles, S. Kim, R. Baughman, Harvesting electrical energy from carbon nanotube yarn twist, *Science* 357 (6353) (2017) 773–778.
- [12] J. Mu, M. Jung de Andrade, S. Fang, X. Wang, E. Gao, N. Li, S.H. Kim, H. Wang, C. Hou, Q. Zhang, M. Zhu, D. Qian, H. Lu, D. Kongahage, S. Talebian, J. Foroughi, G. Spinks, H. Kim, T. Ware, H. Sim, D. Lee, Y. Jang, S. Kim, R. Baughman, Sheath-run artificial muscles, *Science* 365 (6449) (2019) 150–155.
- [13] I. Palaci, S. Fedrigo, H. Brune, C. Klinke, M. Chen, E. Riedo, Radial elasticity of multiwalled carbon nanotubes, *Phys. Rev. Lett.* 94 (17) (2005), 175502.
- [14] M. Yu, T. Kowalewski, R. Ruoff, Investigation of the radial deformability of individual carbon nanotubes under controlled indentation force, *Phys. Rev. Lett.* 85 (7) (2000) 1456–1459.
- [15] W. Lu, M. Zu, J.H. Byun, B. Kim, T. Chou, State of the art of carbon nanotube fibers: opportunities and challenges, *Adv. Mater.* 24 (14) (2012) 1805–1833.
- [16] M. Zu, W. Lu, Q.W. Li, Y. Zhu, G. Wang, T. Chou, Characterization of carbon nanotube fiber compressive properties using tensile recoil measurement, *ACS Nano* 6 (5) (2012) 4288–4297.
- [17] Y. Li, W. Lu, S. Sockalingam, B. Gu, B. Sun, J.W. Gillespie, T.-W. Chou, Electromechanical behavior of carbon nanotube fibers under transverse compression, *J. Phys. D Appl. Phys.* 50 (8) (2017), 085303.
- [18] H. Poritsky, Stresses and deflections of cylindrical bodies in contact with application to contact of gears and of locomotive wheels, *J. Appl. Mech.* 17 (1950) 191–201.
- [19] M. Miao, J. McDonnell, L. Vuckovic, S. Hawkins, Poisson's ratio and porosity of carbon nanotube dry-spun yarns, *Carbon* 48 (10) (2010) 2802–2811.
- [20] U. Anazodo, E. Norris, Effects of genetic and cultural-practices on the mechanical-properties of corn cobs, *J. Agric. Eng. Res.* 26 (2) (1981) 97–107.
- [21] B. Carey, P. Patra, L. Ci, G. Silva, P. Ajayan, Observation of dynamic strain hardening in polymer nanocomposites, *ACS Nano* 5 (4) (2011) 2715–2722.
- [22] A. Agrawal, A. Chipara, Y. Shamoo, P. Patra, B. Carey, P. Ajayan, W. Chapman, R. Verduzco, Dynamic self-stiffening in liquid crystal elastomers, *Nat. Commun.* 4 (2013) 1739.
- [23] Z. Dai, Y. Wang, L. Liu, X. Liu, P. Tan, Z. Xu, J. Kuang, Q. Liu, J. Lou, Z. Zhang, Hierarchical graphene-based films with dynamic self-stiffening for biomimetic artificial muscle, *Adv. Funct. Mater.* 26 (38) (2016) 7003–7010.
- [24] M. Ashby, *Materials Selection in Mechanical Design*, Butterworth-Heinemann, 2011.
- [25] E. Gao, W. Lu, Z. Xu, Strength loss of carbon nanotube fibers explained in a three-level hierarchical model, *Carbon* 138 (2018) 134–142.
- [26] O. Blakslee, D. Proctor, E. Seldin, G. Spence, T. Weng, Elastic constants of compression-annealed pyrolytic graphite, *J. Appl. Phys.* 41 (8) (1970) 3373–3382.